

## Article

# Weakening of Ledinegg Instability and Maldistribution of Boiling Flow in Parallel Microchannels by Entry Effects

Jieyan Jiang <sup>1</sup>, Changxu Chen <sup>1</sup>, Haoxiang Huang <sup>1,2,\*</sup> and Zhenhai Pan <sup>3,\*</sup><sup>1</sup> School of Mechanical Engineering, Shanghai Jiao Tong University, Shanghai 200240, China<sup>2</sup> China Anhui Smagnet Materials Technology Co., Ltd., Fuyang 236000, China<sup>3</sup> School of Mechanical Engineering, Shanghai Institute of Technology, Shanghai 201418, China

\* Correspondence: p461265034@sjtu.edu.cn (H.H.); panzh\_h\_sit@163.com (Z.P.)

**Abstract:** In the pursuit of enhancing thermal management for miniaturized electronic devices, our study delves into the impact of entry effects on Ledinegg instability and flow maldistribution within parallel microchannels. Utilizing a coupled model that incorporates phase change and pressure drop dynamics in boiling flow, we examine microchannels characterized by a 50 length-to-diameter ratio and a 200  $\mu\text{m}$  hydraulic diameter. Our findings unveil a significant influence of entry effects, which narrow the total flow excursion interval, thereby bolstering system stability. Specifically, as the heat flux escalates from 5  $\text{W}/\text{cm}^2$  to 120  $\text{W}/\text{cm}^2$ , the entry effects increasingly mitigate flow instability and maldistribution in parallel channels, diminishing the total flow rate range susceptible to flow instability by 4.73% and 47.52%, while narrowing the total flow rate range corresponding to uneven flow distribution by 4.70% and 46.75%, respectively. Furthermore, entry effects expand the inlet subcooling range necessary for stabilizing the parallel channel system by 38.89% and 1000%. This research not only underscores the importance of considering entry effects in microchannel design but also opens avenues for further exploration into enhancing thermal management solutions.

**Keywords:** microchannel; entry effects; flow boiling; instability



**Citation:** Jiang, J.; Chen, C.; Huang, H.; Pan, Z. Weakening of Ledinegg Instability and Maldistribution of Boiling Flow in Parallel Microchannels by Entry Effects. *Energies* **2024**, *17*, 1901. <https://doi.org/10.3390/en17081901>

Academic Editor: Anastassios M. Stamatelos

Received: 28 February 2024

Revised: 29 March 2024

Accepted: 9 April 2024

Published: 16 April 2024



**Copyright:** © 2024 by the authors. Licensee MDPI, Basel, Switzerland. This article is an open access article distributed under the terms and conditions of the Creative Commons Attribution (CC BY) license (<https://creativecommons.org/licenses/by/4.0/>).

## 1. Introduction

Rapid technological advancements in fields such as integrated circuits, nuclear reactors, and medical instruments necessitate more efficient cooling techniques [1]. Researchers are seeking solutions to address the challenges of heat dissipation in miniaturized electronic devices, where heat flux varies from 100 to 1000  $\text{W}/\text{cm}^2$ . Microchannel heat exchangers have proven to offer compact structures, high efficiency of heat transfer, and uniform wall temperature distribution [2,3]. However, boiling flow in microchannels is subject to various flow instabilities caused by transitions in flow patterns and liquid backflow. Among these instabilities, Ledinegg instability is particularly noteworthy. This instability occurs when the flow deviates from its initial equilibrium state following a certain disturbance, stabilizing again at a different flow rate [4].

For clearer understanding of Ledinegg instability, assume the channel pressure drop as a function of mass flux under constant heat input. Such a channel load curve, along with a general pump curve, is displayed in Figure 1. For a heated channel, vapor begins to generate as the flow rate decreases below the onset of nucleate boiling, causing both friction and acceleration pressure drop to increase rapidly. Once the channel is nearly filled with vapor, the pressure drop decreases again as the flow reverts back to single-phase. Therefore, the load curve of a heated channel is not monotonic like that of an adiabatic channel. In cases when a general pump is applied to the channel inlet, steady-state operating conditions only occur where the pump curve intersects with the channel load curve, such as at points B, D, and F. These points represent potential operational scenarios under a standard pump curve with varying flow rates. The equivalence of pressure drop of these points results

in the possible occurrence of uneven flow distribution within a parallel channel system. For an individual channel, the operating condition at point D will drift to point B or point F under minor fluctuations in flow rate. Such flow rate excursion occurs when the slope of the channel load curve is algebraically smaller than the pump curve and is defined by Ledinegg [5] as Ledinegg instability, which can lead to flow maldistribution among parallel microchannels and localized deterioration of heat transfer within the heat exchanger [6].

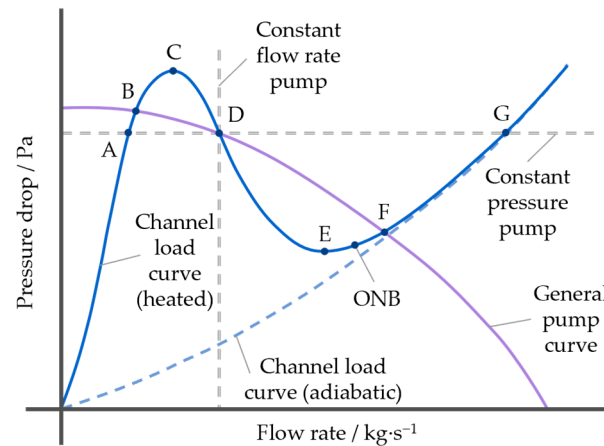


**Figure 1.** Schematic diagram of Ledinegg instability. ONB denotes the onset of nuclear boiling.

Extensive research has been conducted on the phenomenon of Ledinegg instability, focusing on conducting quantitative experimental analysis and developing mathematical models for the pressure drop. Initially, different quantities flowing through parallel-connected tubes were observed despite approximately equal heating [5]. Results obtained in the experiment suggest that once a tube somehow contains less working fluid than the others, vapor will possibly generate, causing an increase in flow resistance and thus a decrease in heat dissipation. Consequently, the flow rate continues to decrease until it reaches a new equilibrium state. The appearance of such instability was verified to be related to the non-monotonicity of the boiling flow pressure drop curve. Subsequently, research has demonstrated that the distributions of flow rates, their hysteresis, and the onset of excursion phenomena in parallel systems can be estimated from pressure drop versus flow rate curves in single tubes [7,8]. Ledinegg instability and uneven distribution occur when the characteristic curve exhibits negative tangents, despite the approximate similarity of the curves of each tube. Further, the onset of flow instability (OFI) is defined as the occurrence of a minimum in the pressure drop curve (point E in Figure 1) [9], associated with a constant pressure pump. For general pumps, stability judgment is made based on the relative magnitude of the partial derivatives at the current operating point.

On the basis of mechanistic studies, experiments have been conducted to investigate the parametric effects on the occurrence and sensitivity of Ledinegg instability. It has been revealed that the inlet flow excursion becomes more pronounced under higher exit quality and can be suppressed by entrance throttling [10], but it lacks quantitative analysis of the extent of Ledinegg instability [10]. Thus, the slope's magnitude in the negative slope region is subsequently determined as the significance criterion. Parametric studies evaluated by this criterion indicate that Ledinegg instability can be weakened and even avoided at lower power input, larger hydraulic diameter, and higher system pressure [11,12]. There have been many other similar experimental studies within the last few decades, assembling a huge database of channel pressure drops and instabilities [13–15], laying the groundwork for numerical studies to predict channel pressure drop and stability forecast.

Considering the complexity of bubble generation and flow pattern transformations, simplified pressure drop models for boiling flow within the microchannel need to be developed. Initially, the Martinelli–Nelson correlation, which employs separated single-phase flow assumption and an equivalent Reynolds number for simplification, was proposed [16]

for forced turbulent flow in a general-size tube. Simplification was performed through separate evaluation of the friction and acceleration pressure gradient. However, pressure drops calculated using this correlation show bias compared to the measured values, owing to limited experimental validation. By introducing a hydraulic parameter into the model, the Lockhart–Martinelli correlation achieved better accuracy for laminar boiling flow in macro channels [17]. When applied to microchannel laminar flow, the above two models exhibit a large deviation in calculated pressure drops compared to experimental results, indicating the necessity of modification accordingly for size effects. By incorporating the hydraulic diameter, the Mishima–Hibiki correlation shows higher accuracy for the pressure drop of microchannels [18]. Nevertheless, application limitations still exist, as the model does not independently address the pressure drop of two-phase flow. The Muzychka–Award correlation mitigates this issue by defining the two-phase flow pressure drop as a linear combination of three simple pressure drops or pressure gradients, namely single-phase liquid, single-phase vapor, and interfacial pressure drop [19]. This method improves the flexibility and adaptability of the model to various operating conditions.

System stability and flow distribution can be investigated based on the obtained channel load curve. The latter is simply combinations of intersections between the channel load curve and the pump curve, while the former requires complex data processing. The mainstream analysis method consists of the Chebyshev collection method [20,21], the perturbation analysis method [22], and system linearization [7]. With reference to the experimental results, Akagawa et al. indicates that instability is not bound to occur when one channel in a parallel system operated in the negative tangent region [7]. Also, stability criteria for system consisting of 1~3 channels were proposed by linearizing the force balance equations and performing a Laplace transformation with a similar methodology to Reich [23]. The stability issue of parallel multi-channel systems is transformed into an eigenvalue problem, thereby proposing criteria for the occurrence of system flow instability. Asymptotic stability behavior as the number of parallel channels increases to dozens is investigated using a similar method [24].

With the rapid miniaturization and integration of microelectronic devices, microchannel heat sinks are faced with fast-growing design requirements for reduced volume and increased specific surface area. Since the minimum hydraulic diameter of the channel is constrained by fluid dynamics, the length-to-diameter ratio will continue to shrink, leading to non-negligible deviation contributing to channel scaling effects [25]. Current research for boiling flow instability is predominantly conducted with fully developed assumptions. Prediction and discussion of flow instability and uneven distribution of developing flow are virtually uncharted, indicating potential limitations of optimizing flow boiling heat exchangers in miniaturized industrial applications.

This study aims to perform a theoretical investigation of impact-of-entry effects on Ledinegg instability and flow maldistribution in developing flows associated with phase change. The channels are specified with a small length-to-diameter ratio. All results are presented and compared under two circumstances: considering entry effects and assuming fully developed flow. The channel pressure drop is calculated using a separated flow model, and the flow instability characteristics are discussed using a linear analysis of the dynamic system. The impact of the entry effects on the model is introduced by adjusting the friction factor in the model. Parametric analysis is conducted, focusing on the channel length-to-diameter ratio, flow rate, heat flux, and inlet subcooling. Our objective is to elucidate the mechanism of the impact-of-entry effects on flow instability in parallel microchannels and provide a theoretical basis for the miniaturized heat exchanger design.

## 2. Models and Methods

### 2.1. Problem Description

The schematic layout of the system is shown in Figure 2. This study examines a parallel channel system cooperating with a constant pressure pump. Water serves as the working fluid. Each channel has both width and height measuring 0.0002 m. The system is supplied

with fluid at a fixed mass flow rate ( $W$ ) and a constant pressure outlet ( $p_{out} = 101,325$  Pa). The microchannels are thermally isolated from each other. Uniform heat fluxes ( $q$ ) are applied to the channels' wall. The thermal resistance of the wall is neglected to simplify the solution for the energy equation.

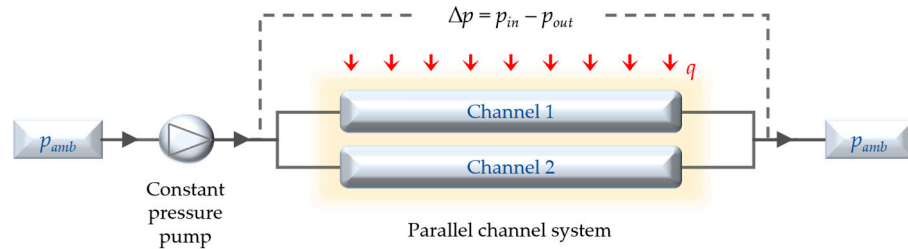


**Figure 2.** Schematic layout of parallel channel system.  $p_{amb}$  denotes the ambient pressure ( $p_{out} = p_{amb}$ ).

As stated in Figure 1, the exploration of Ledinegg instability is founded on the pump curve and channel load curve, which is calculated through the mathematical modeling method in this study. On the basis of the channel load curve, the flow distribution and system stability between parallel channels are analyzed through database traversal and linearization of system dynamics.

Since the entry effects essentially affect the channel pressure drop, the first step in our investigation is to calculate the pressure drop under different hydrodynamic hypotheses: (1) considering entry effects; (2) assuming fully developed flow along the entire channel. Pressure drop models for developing and fully developed flow need to be proposed and validated separately. In particular, in order to investigate the impact of entry effects, especially on channels with small length-to-diameter ratios ( $x^*$ ), it is necessary to determine a suitable channel length. Based on the preceding discussion, the modeling and stability analysis methods adopted in our work are presented in the following sections.

Further, parametric studies are designed to assess the significance of the impact of entry effects under different operating conditions. Four types of variables are considered in this study: channel length-to-diameter ratio ( $x^*$ ), heat flux ( $q$ ), mass flow rate ( $W$ , corresponding to  $Re$ ), and inlet temperature ( $T_{in}$ , corresponding to  $\Delta T_{sub}$ ). Specific values for each variable will be provided in the results section.

## 2.2. Model Derivation

In this study, we adopted a two-phase separated flow model for pressure drops in microchannels. As proposed by Lockhart et al. [17,24], the conservation equations for mass, momentum, and energy within a single microchannel are delineated as follows:

$$\frac{\partial G}{\partial x} = 0 \quad (1)$$

$$\frac{\partial}{\partial x} \left[ \left( \frac{v_f(1-\sigma)^2}{1-\alpha} + \frac{v_g\sigma^2}{\alpha} \right) G^2 \right] = -\frac{\partial p}{\partial x} - F_w \quad (2)$$

$$\frac{\partial}{\partial x} (hG) = \frac{q'}{A} \quad (3)$$

where  $G$  is the mass flux ( $\text{kg} \cdot \text{m}^{-2} \cdot \text{s}^{-1}$ );  $x$  is the axial position (m);  $p$  is the pressure (Pa);  $v_f$  and  $v_g$  are the specific volumes of water and steam ( $\text{m}^3/\text{kg}$ );  $A$  is the channel cross-sectional area ( $\text{m}^2$ );  $\sigma$  is the vapor quality;  $h$  is the fluid-specific enthalpy ( $\text{J}/\text{kg}$ );  $q'$  is the heat input per unit length ( $\text{W}/\text{m}$ ).

The underlying assumption of Equation (2) is proposed by Martinelli et al. [16] and depicted in Figure 3. With sufficient heat flux applied to the channel, the subcooled working fluid can always start boiling and transition into superheated vapor at any location. Given this observation, the channel can be equivalently divided into several flow parts along the

axial direction. In each part of the microchannel, i.e., liquid phase part ( $\sigma = 0$ ), liquid–vapor two-phase part ( $0 < \sigma < 1$ ), and vapor phase part ( $\sigma = 1$ ), the pressure gradient  $\partial p / \partial x$  can be independently calculated by Equation (2) by incorporating the local value of  $\sigma$ .

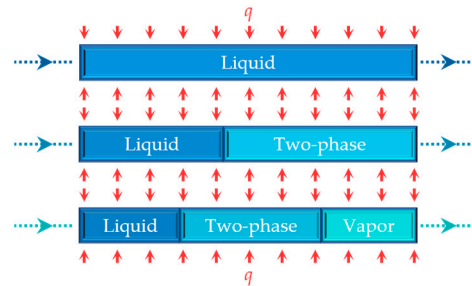


**Figure 3.** Layout of separated flow assumption.

Boundary conditions are defined as follows:

$$G|_{inlet} = G_{in} \quad (4)$$

$$p|_{outlet} = p_{out} \quad (5)$$

$$h|_{inlet} = h(T_{in}, p_{amb}) \quad (6)$$

Using the finite volume method, the pressure drop in the channel can be solved from conservation Equations (1) to (3) with specified boundary conditions.

The vapor quality  $\sigma$  and vapor volume fraction  $\alpha$  are defined as follows:

$$\sigma = \max \left\{ \frac{h - h_f}{h_g - h_f}, 1 \right\} \quad (7)$$

$$\alpha = \frac{1}{1 + \frac{v_f}{v_g} S \frac{1-\sigma}{\sigma}} \quad (8)$$

where  $h_f$  and  $h_g$  are the specific enthalpy of saturated liquid and vapor (J/kg).

The slip ratio  $S$  is defined as follows according to Zivi et al. [26]:

$$S = \left( \frac{v_g}{v_f} \right)^{\frac{1}{3}} \quad (9)$$

The empirical correlation introduced by Muzychka et al. [19] is used to calculate the friction pressure gradient  $F_w$ :

$$F_w = \left( \frac{\partial p}{\partial x} \right)_f + C \sqrt{\left( \frac{\partial p}{\partial x} \right)_f \left( \frac{\partial p}{\partial x} \right)_g} + \left( \frac{\partial p}{\partial x} \right)_g \quad (10)$$

where the first and third term denote the single-phase frictional pressure gradient, i.e., it is assumed that no second phase exists:

$$\left( \frac{\partial p}{\partial x} \right)_f = 2f_f \frac{v_f (1 - \sigma)^2 G^2}{D} \quad (11)$$

$$\left( \frac{\partial p}{\partial x} \right)_g = 2f_g \frac{v_g \sigma^2 G^2}{D} \quad (12)$$

where:  $f$  is the Fanning friction factor;  $D$  is the hydraulic diameter (m).

The length-to-diameter ratio  $x^*$  is defined as the ratio of the axial channel length to the hydraulic diameter:

$$x^* = \frac{L}{D} \quad (13)$$

Subsequently, the formula for the friction factor  $f$  for fully developed flow is derived. According to Acrivos et al. [27], the friction pressure drop  $P$  and friction factor  $f$  can be written in terms of:

$$P = \frac{2f\rho u^2 x}{D} \quad (14)$$

$$f = \frac{\tau_w}{(1/2)\rho u^2} \quad (15)$$

where  $\rho$  and  $u$  are the fluid density ( $\text{kg}/\text{m}^3$ ) and velocity ( $\text{m}/\text{s}$ );  $\tau_w$  is the wall shear stress (Pa).

For the friction factor for fully developed laminar flow in a rectangular channel, an empirical equation is presented as follows according to Shah et al. [28]:

$$f = \frac{24}{Re} \left( 1 - 1.3553\beta + 1.9467\beta^2 - 1.7012\beta^3 + 0.9564\beta^4 - 0.2537\beta^5 \right) \quad (16)$$

where  $\beta$  is the microchannel aspect ratio.

This pressure drop model is a prevalent framework extensively employed to analyze boiling phenomena within microchannel flows. Subsequently, the derivation of the formula for the apparent friction factor, as proposed by Shah [29], accounting for the entry effects, is outlined below.

According to Equation (14), the relationship between the apparent friction factor  $f_A$  and the apparent pressure drop  $P_A$  can be rewritten as follows:

$$f_A = \frac{P_A D}{2\rho u^2 x} \quad (17)$$

Define dimensionless hydrodynamic length  $x^+$  as:

$$x^+ = \frac{x}{DRe} \quad (18)$$

Substitute  $x^+$  to Equation (17):

$$f_A Re = \frac{P_A D Re}{2\rho u^2 x} = \frac{P_A}{2\rho u^2 x^+} \quad (19)$$

The dimensionless apparent pressure drop  $P_A^*$  is defined as follows:

$$P_A^* = \frac{P_A}{\rho u^2 / 2} = (f_A Re)(4x^+) = (f Re)(4x^+) + K(x^+) \quad (20)$$

where  $K(x^+)$  is separated as the additional dimensionless apparent pressure drop. For flow that has achieved full development, it is posited that  $K(x^+)$  converges to  $K(\infty)$ . In this case, the dimensionless pressure drop  $P_A^*$  can be expressed as:

$$P_A^* = (f Re)(4x^+) + K(\infty) \quad (21)$$

Researchers have conducted extensive experimental studies to adopt empirical expressions for Equation (21). Specifically, Shapiro and Bender et al. [30,31] derived the following equations for  $P_A^*$  over the whole range of  $x^+$  through experimental investigation:

$$\begin{aligned} P_A^* &= 13.74\sqrt{x^+} & x^+ &\in [10^{-5}, 10^{-3}] \\ P_A^* &= 1.25 + 64x^+ & x^+ &\geq 0.06 \end{aligned} \quad (22)$$

Based on their framework, Shah [29] proposed the following correlation to predict  $f_A Re$  for laminar flow in microchannels:

$$f_A Re = \frac{3.44}{\sqrt{x^+}} + \frac{(fRe) + K(\infty)/(4x^+) - \frac{3.44}{\sqrt{x^+}}}{1 + C(x^+)^{-2}} \tag{23}$$

where  $K(\infty)$  and  $C$  are geometric factors related only to the channel cross-section shape and aspect ratio. In this study, the correlation for  $f_A$  can be specified as follows according to Curr et al. [32]:

$$f_A = \frac{1}{Re} \left( \frac{3.44}{\sqrt{x^+}} + \frac{14.227 + \frac{1.43}{4x^+} - \frac{3.44}{\sqrt{x^+}}}{1 + 0.00029(x^+)^{-2}} \right) \tag{24}$$

In the entrance region, where both velocity and pressure gradient are heightened, the pressure drop associated with developing flow exceeds that of fully developed flow. Consequently, a definitive point marking the length distinction emerges between developing and fully developed flows. This is also a transition point for the application of different friction factors in our pressure drop model. The empirical correlation equation introduced by Duan et al. [33] is used to define the entrance region length of a microchannel, which serves as the transition point in our work:

$$L_e = \left( \frac{0.74}{0.09Re + 1} + 0.0889Re \right) D \tag{25}$$

### 2.3. Flow Instability Criterion

According to Akagawa et al. [7], the equations for the force balance in each channel and the continuity between parallel channels can be listed as follows:

$$\begin{cases} P_p(W) = P_1(W_2) + m_1 \frac{dW_1}{dt} \\ \quad \quad \quad = P_2(W_2) + m_2 \frac{dW_2}{dt} \\ W = \sum_{i=1}^n W_i \end{cases} \tag{26}$$

where  $P_p$  is the pressure head of the pump;  $P_i$  ( $i = 1, 2$ ) and  $W_i$  ( $i = 1, 2$ ) are the pressure drop and mass flow rate in each microchannel;  $W$  is the total flow rate of the system;  $t$  is the time coordinate;  $m_i$  ( $i = 1, 2$ ) is the inertia coefficient of each channel:

$$m_i = m = \frac{L}{A} \tag{27}$$

The linearization of this system is presented as follows, referring to Van et al. [24]:

$$\begin{bmatrix} m_1 & & & \\ & m_2 & & \\ & & 0 & \\ & & & 0 \end{bmatrix} \cdot \frac{d}{dt} \begin{bmatrix} \delta W_1 \\ \delta W_2 \\ \delta W \\ \delta(\Delta p) \end{bmatrix} = \begin{bmatrix} -\varepsilon_1 & & & 1 \\ & -\varepsilon_2 & & 1 \\ & & \varepsilon_p & \varepsilon_{\Delta p} \\ 1 & 1 & -1 & 0 \end{bmatrix} \cdot \begin{bmatrix} \delta W_1 \\ \delta W_2 \\ \delta W \\ \delta(\Delta p) \end{bmatrix} \tag{28}$$

where  $\varepsilon$  denotes the partial derivatives as follows:

$$\varepsilon_i = \frac{\partial P_i}{\partial W_i}, \quad i = 1, 2 \tag{29}$$

$$\varepsilon_p = \frac{\partial P_p}{\partial W} \tag{30}$$

$$\varepsilon_{\Delta p} = \frac{\partial P_p}{\partial(\Delta p)} \tag{31}$$

For a constant pressure pump applied in this study,  $\varepsilon_p = 0$ . Rewrite Equation (28) into a set of characteristic equations:

$$(\lambda m_i + \varepsilon_i) \mathbf{v}_i = 0, \quad i = 1, 2 \tag{32}$$

$$\left( \sum_{i=1}^n \mathbf{v}_i \right) - \mathbf{v}_p = 0 \tag{33}$$

where  $\mathbf{v}_i$  is the eigenvector corresponding to each channel;  $\mathbf{v}_p$  is the eigenvector corresponding to the pump;  $\lambda$  is the eigenvalue of each characteristic equation. This system has two eigenvalues, respectively:

$$\lambda \in \left\{ -\frac{\varepsilon_i}{m_i} \right\} \tag{34}$$

The inertia coefficient  $m$  is a geometric parameter, i.e.,  $m > 0$ , and  $\varepsilon$  is equivalent to the slope of the channel load curve. The stability criterion for the system can be defined as follows:

$$k = \sum_{i=1}^n \left( -\frac{\varepsilon_i}{m_i} \right) \tag{35}$$

As a constant pressure pump (with a pressure curve slope of 0) is used in this system, the stable operating point of the parallel two-channel system appears only when the sum of the slopes of the channel pressure drop curves exceeds zero, i.e.,  $k \leq 0$ , according to Akagawa et al. [7].

#### 2.4. Model Validation

Figures 4 and 5 provide a comparison of our results with previous literature data. Operating conditions for each validation are listed in Table 1.

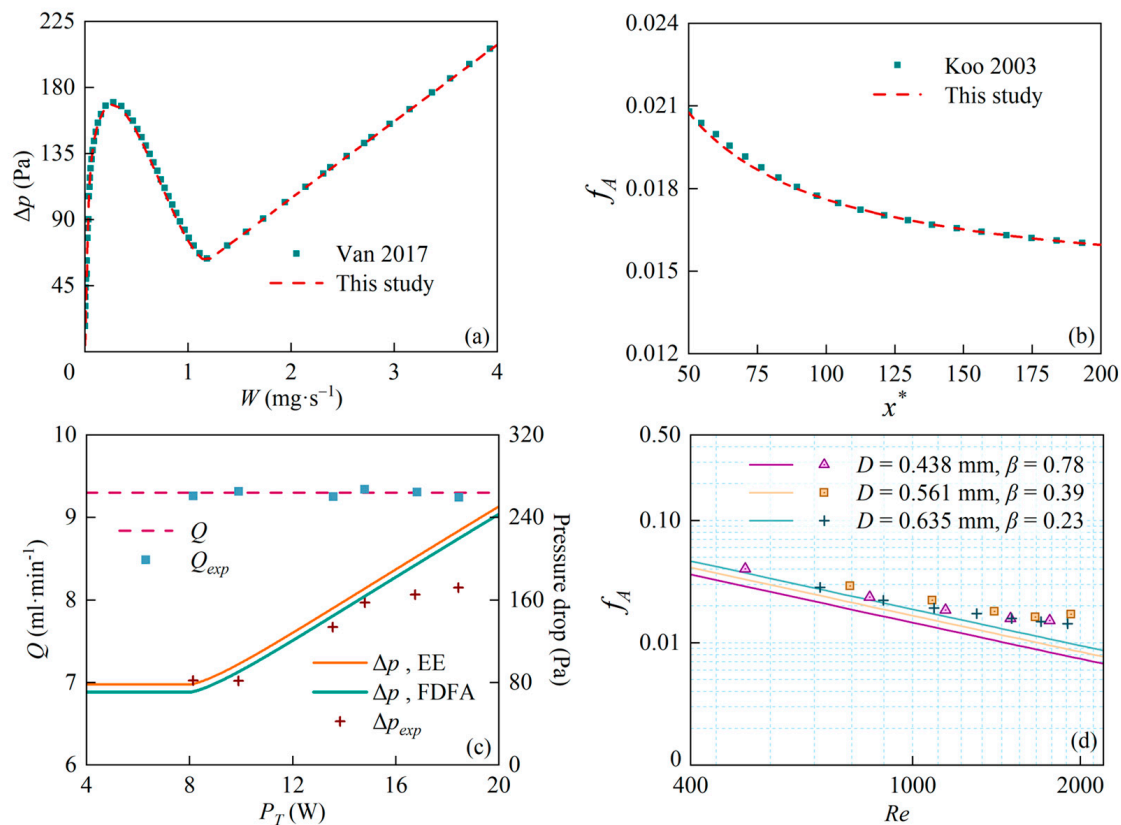


**Figure 4.** Comparison with literature data: (a) pressure drop with Ref. [24]; (b) apparent friction factor with Ref. [34]; (c) pressure drop with Ref. [35]; (d) apparent friction factor with Ref. [36].

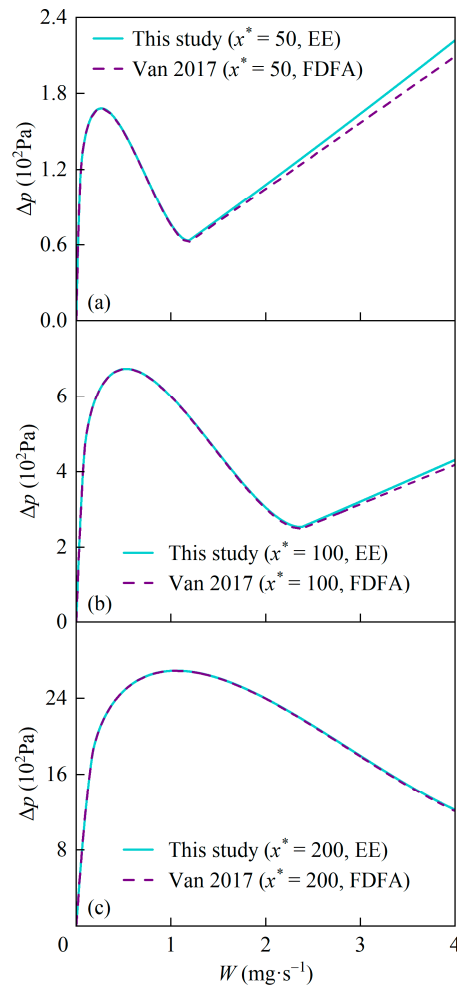


**Figure 5.** Significance of entry effects in comparison with literature data with Ref [24] at: (a)  $x^* = 50$ ; (b)  $x^* = 100$ ; (c)  $x^* = 200$ . EE denotes the case considering entry effects, while FDFA denotes the case assuming fully developed flow.

**Table 1.** Operating conditions for model validation.

Figure	Ref	$\Delta p/f_A$	$N^2/E^3$	Length	D/mm	$\beta$	Heat Load	Flow Rate	$T_{in}/K$
Figure 4a	Ref. [24]	$\Delta p$	N	L: 0.01 m	0.2	1	5 W/cm <sup>2</sup>	W: 0~4 mg/s	353.15
Figure 4b	Ref. [34]	$f_A$	N	$x^*$ : 50~200	/	1	/	Re: 1000	/
Figure 4c	Ref. [35] <sup>1</sup>	$\Delta p$	E	L: 0.11 m	1	1	4~20 W	Q: 9.3 mL/min	361.65
Figure 4d	Ref. [36]	$f_A$	E	L: 0.062 m	0.438 0.635	0.78 0.69	/	Re: 400~2200	/
Figure 5a	Ref. [24]	$\Delta p$	N	$x^*$ : 50	0.2	1	5 W/cm <sup>2</sup>	W: 0~4 mg/s	353.15
Figure 5b	Ref. [24]	$\Delta p$	N	$x^*$ : 100	0.2	1	5 W/cm <sup>2</sup>	W: 0~4 mg/s	353.15
Figure 5c	Ref. [24]	$\Delta p$	N	$x^*$ : 200	0.2	1	5 W/cm <sup>2</sup>	W: 0~4 mg/s	353.15

<sup>1</sup> Reference data are conducted over a single channel except for Ref. [35] (two parallel channels). <sup>2</sup> N denotes numerical study. <sup>3</sup> E denotes experimental study.

Specifically, Figure 4a,b presents a comparison with numerical results, while Figure 4c,d displays a comparison with experimental data. It is noteworthy in Figure 4c that the pressure drop obtained through our model directly with power input  $P_T$  is slightly higher than the experimental result, since the exact fluid heat absorption was reduced due to thermal resistance and power loss. Further, it is indicated from Figure 4d that Equation (24) is more accurate for laminar flows. As depicted in the figure, the results of pressure drop and apparent friction factor align well with both numerical and experimental references, indicating the effectiveness of our method.

It is worth emphasizing that Van et al. [24] obtained the pressure drop with  $x^*$  of 50 based on the assumption of fully developed flow. Utilizing their mathematical model and operating conditions, the microchannel pressure drops at  $x^*$  of 100 and 200 were calculated as extended data from the literature, as depicted in Figure 5. Comparison in the figure suggests that as  $x^*$  increases, the sensitivity of the pressure drop model to the apparent friction factor  $f_A$  decreases, indicating a diminished impact of entry effects. This observation aligns with the established principles of fluid dynamics development.

### 3. Results and Discussion

#### 3.1. Impact of Entry Effects on Flow Instability and Maldistribution

Figure 6 presents the comparison between  $f$  and  $f_A$ . Results are conducted with  $x^*$  ranging from 1 to 200 and  $Re$  set at 50/100/200, respectively. As depicted in the figure, the relative deviation between these two friction factors increases with decreasing  $x^*$  due to a greater pressure gradient. Additionally,  $f_A$  converges towards  $f$  at a diminished rate as  $Re$  increases. For a microchannel operating under larger  $Re$ , it is necessary to increase  $x^*$  to directly substitute  $f_A$  with  $f$  (i.e., to apply the assumption of fully developed flow to the entire channel).

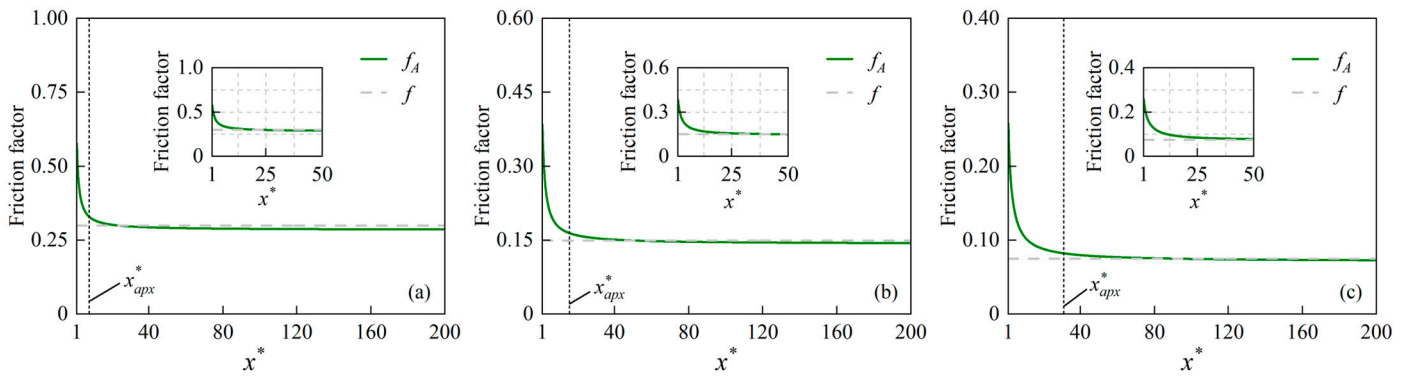


Figure 6. Friction factors at: (a)  $Re = 50$ ; (b)  $Re = 100$ ; (c)  $Re = 200$ .

To clearly illustrate the converging rate between these two friction factors, we introduce an approximate converging ratio as:

$$x^*_{apx} = x^* |_{f_A/f=1.1} \tag{36}$$

It is evident that  $x^*_{apx}$  represents the characteristic length-to-diameter ratio, which denotes the relative approximation between  $f$  and  $f_A$ . Values of  $x^*_{apx}$  under various  $Re$  are listed in Table 2. Regarding these  $x^*_{apx}$ , the channel length-to-diameter ratio,  $x^*$ , is set to 50 in the following sections (i.e., the channel length is set as 0.01 m).

Table 2. Approximate converging ratio  $x^*_{apx}$  at different  $Re$ .

$Re$	$x^*_{apx}$
50	7.75
100	15.5
200	31

Applying  $f_A$  and  $f$  to the model, the pressure drops and flow distribution ( $R_i = W_i/W$ ) within the system are obtained. Operating conditions include an inlet temperature of 353.15 K and heat fluxes of 5 W/cm<sup>2</sup> and 120 W/cm<sup>2</sup>, respectively. For different heat fluxes, mass flow rate is specified in ranges of 0~5 mg/s and 0~120 mg/s, corresponding to  $Re$  ranging within 0~71 and 0~1694. Additionally, by processing the linearization analysis, the occurrence of flow instability is also depicted in Figures 7 and 8.

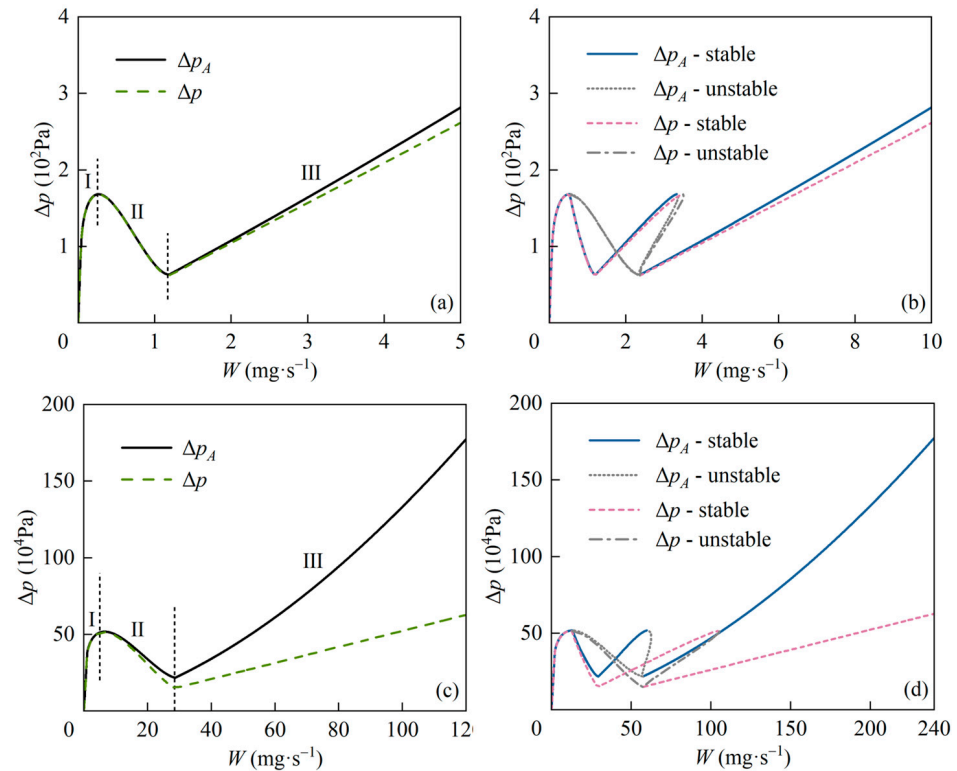


**Figure 7.** Pressure drops and unstable operating points of individual channel and parallel channels at different heat fluxes: (a)  $q = 5 \text{ W/cm}^2$ , individual channel; (b)  $q = 5 \text{ W/cm}^2$ , parallel channels; (c)  $q = 120 \text{ W/cm}^2$ , individual channel; (d)  $q = 120 \text{ W/cm}^2$ , parallel channels.

As displayed in Figure 7a,c, each channel load curve is divided into three distinct regions (Zone I, Zone II, and Zone III) based on changes in slope. Zone II represents the two-phase flow zone, characterized by a negative slope of the curve. Conversely, Zones I and III represent combinations of two-phase flow with pure steam and pure liquid flow (since there are slight deviations between the flow transition points and the slope transition points), each exhibiting a positive slope.

Figure 7a,c illustrates that the entry effects significantly increase the pressure drops as flow rate increases, especially in Zone III. This suggests that entry effects have a greater impact on flows dominated by the liquid phase. As the flow rate increases, the deviation between the pressure drops—considering entry effects and assuming a fully developed flow—becomes more pronounced.

All possible flow rate combinations between parallel channels are depicted in Figure 7b,d. According to Section 2.3, flow instability will only occur in the combined case when at least one channel is operating in Zone II. The pressure drop curves of a single channel in Figure 7 reveal that the absolute slope values decrease sequentially from Zone I to Zone III. By referring to the instability criteria described in Section 2.3, the combined operating conditions of II + II and II + III are unstable.

As noted earlier, the entry effects increase the pressure drop, especially for the liquid phase, thus narrowing the possible flow rate range of the channel under a given pressure drop. The reduction is mainly brought about by Zone III. As a result, the total flow rate range for flow instability to occur is also reduced compared to the fully developed flow assumption. For heat fluxes of  $5 \text{ W/cm}^2$  and  $120 \text{ W/cm}^2$ , the entry effects can reduce the total flow rate range for unstable operation by 4.73% and 47.52%, respectively. Detailed data are listed in Table 3.

Figure 8 shows the flow distribution  $R_i$  of every possible combination in the parallel channel system. The horizontal unstable region is associated with the II + II combination, whereas the vertical unstable region corresponds to the II + III combination. As depicted

in the figure, the entry effects significantly reduce the flow rate range of uneven flow distribution in the vertical direction. This observation suggests that the entry effects significantly mitigate the issue of uneven flow distribution in scenarios involving Zone III. For heat fluxes of 5 W/cm<sup>2</sup> and 120 W/cm<sup>2</sup>, the entry effects can reduce the total flow rate range of flow maldistribution by 4.70% and 46.75%, respectively, compared with the fully developed flow assumption. Detailed data are also listed in Table 3.

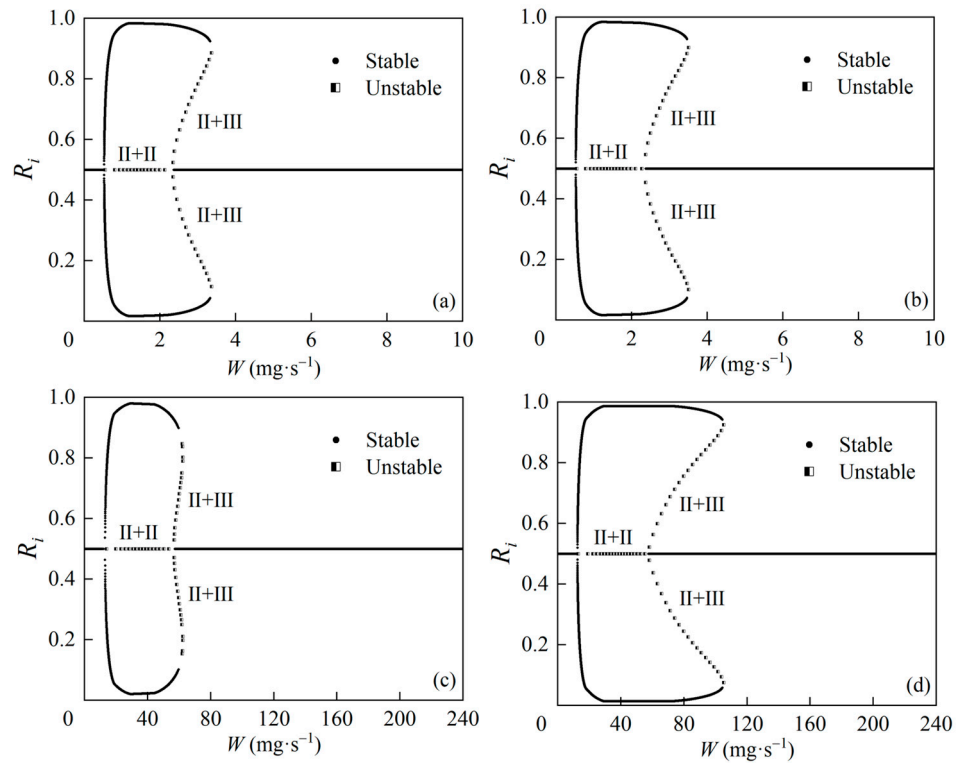


**Figure 8.** Flow rate distribution and unstable operating point under different heat fluxes: (a)  $q = 5 \text{ W/cm}^2$ , considering entry effects; (b)  $q = 5 \text{ W/cm}^2$ , assuming fully developed flow; (c)  $q = 120 \text{ W/cm}^2$ , considering entry effects; (d)  $q = 120 \text{ W/cm}^2$ , assuming fully developed flow.

**Table 3.** Flow rate range of flow instability and maldistribution at different heat fluxes.

		Unstable Region (mg/s)	Reduction Proportion	Unstable Region (mg/s)	Reduction Proportion
$q = 5 \text{ W/cm}^2$	EE <sup>1</sup>	0.55~3.37	4.73%	0.53~3.37	4.70%
	FDFA <sup>2</sup>	0.55~3.51		0.53~3.51	
$q = 120 \text{ W/cm}^2$	EE	14.06~62.46	47.52%	13.09~62.46	46.75%
	FDFA	13.09~105.31		12.59~105.31	

<sup>1</sup> EE denotes the case considering entry effects. <sup>2</sup> FDFA denotes the case assuming fully developed flow.

### 3.2. Impact of Entry Effects on Hazardous Boundary and Critical Subcooling

According to Zhang and Manavela et al. [8,12,37], inlet subcooling is also an important parameter affecting boiling flow instability. Although the dimensionless subcooling number  $N_{sub}$  and phase change number  $N_{pch}$  are generally used in discussions of boiling flow instability, we opt to present our results using the inlet subcooling ratio  $N_{in}$  and heat absorption ratio  $N_{out}$ , as defined below:

$$\begin{cases} N_{sub} = \frac{h_f - h_{in}}{h_{fg}} \frac{\rho_l - \rho_g}{\rho_g} \\ N_{pch} = \frac{q' L}{h_{fg} W} \frac{\rho_l - \rho_g}{\rho_g} \end{cases} \quad \begin{cases} N_{in} = \frac{h_f - h_{in}}{h_{fg}} \\ N_{out} = \frac{q' L}{h_{fg} W} = \frac{h_{out} - h_{in}}{h_{fg}} \end{cases} \quad (37)$$

where:  $h_{fg}$  is the latent heat of vaporization of water (J/kg).  $N_{in}$  denotes the relative vaporization margin at the inlet of the microchannel, while  $N_{out}$  denotes the heat absorption relative to latent heat of vaporization.  $N_{in}$  and  $N_{out}$  are the normalized expression of  $N_{sub}$  and  $N_{pch}$ , facilitating more intuitive discussion in this study.

Figure 9 depicts the boundary points of Zone II (in terms of  $N_{out}$ ) at various inlet temperatures (in terms of  $N_{in}$ ), representing the range of relative heat absorption in the unstable operating region.

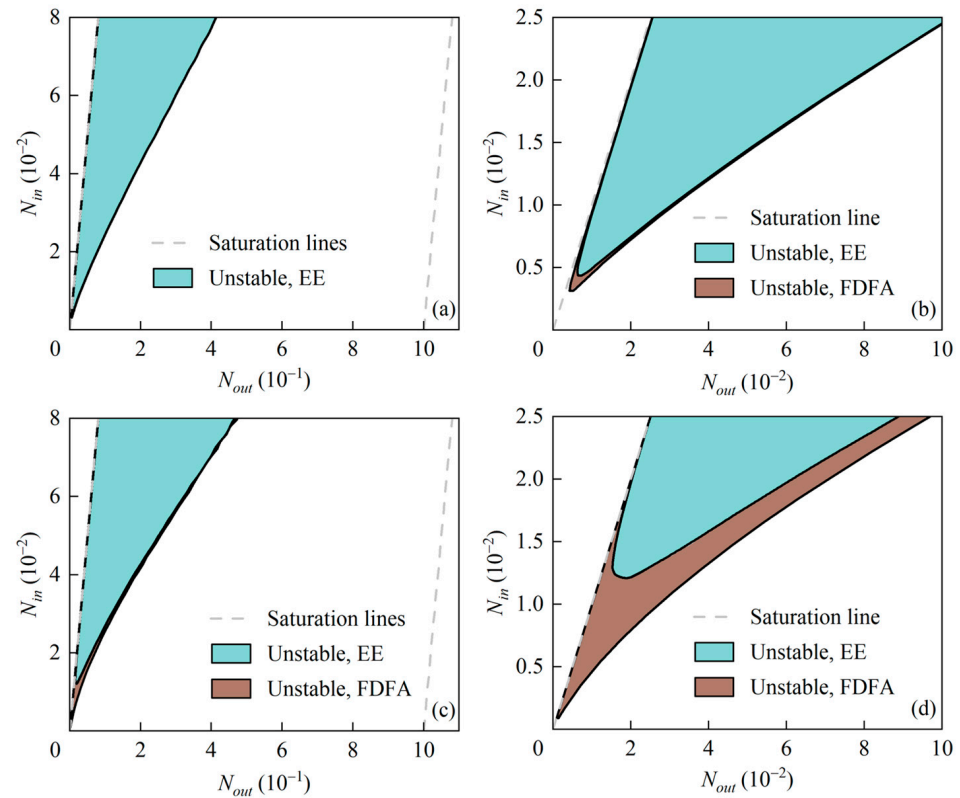


**Figure 9.** Hazardous boundary at different heat fluxes: (a)  $q = 5 \text{ W/cm}^2$ ; (b)  $q = 5 \text{ W/cm}^2$ , zoom in; (c)  $q = 120 \text{ W/cm}^2$ ; (d)  $q = 120 \text{ W/cm}^2$ , zoom in. EE denotes the case considering entry effects, while FDFA denotes the case assuming fully developed flow.

The two dashed lines in Figure 9, representing  $N_{in} = N_{out}$  and  $N_{out} = 1$ , respectively, correspond to saturated liquid and saturated vapor at the outlet. The area between these lines signifies conditions in which the working fluid at the outlet is in a two-phase flow state. As shown in the figure, all the unstable regions are located between the two saturation lines, suggesting that flow instability can only occur when the channel operates with two-phase flow. Such an unstable region corresponds to the area where  $N_{out} > N_{in}$ , indicating vapor generation.

Figure 9 indicates that the flow instability region expands as  $N_{in}$  increases, consistent with the findings of Van et al. [24] and Manavela et al. [8]. Compared to the fully developed flow assumption, entry effects can narrow the thermodynamic range of flow instability. Effects are more pronounced at higher heat fluxes.

For a given channel with fixed heat flux, there exists a critical subcooling ratio, which is the smallest  $N_{in}$  of the hazardous boundary. When the inlet subcooling is below this critical value, the system remains invariably stable since there is mainly vapor flow in the channel. To clarify the underlying mechanism of critical subcooling ratio, pressure drop curves under various  $N_{in}$  are depicted in Figure 10. As  $N_{in}$  decreases, the slope in Zone II becomes progressively flatter and tends toward zero. With reference to Chiapero et al. [37], the mechanism of this transition can be explained as follows.

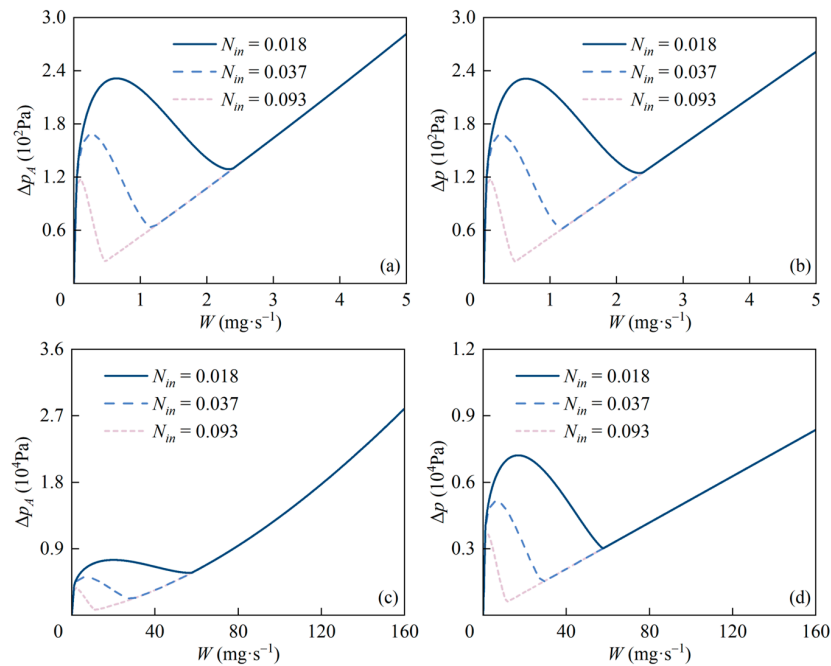


**Figure 10.** Pressure drop curves at different  $N_{in}$  and heat fluxes: (a)  $q = 5 \text{ W/cm}^2$ , considering entry effects; (b)  $q = 5 \text{ W/cm}^2$ , under fully developed flow assumption; (c)  $q = 120 \text{ W/cm}^2$ , considering entry effects; (d)  $q = 120 \text{ W/cm}^2$ , under fully developed flow assumption.

The thermodynamic quality (in the thermodynamic equilibrium approximation) at the channel outlet is defined as:

$$x_{out} = \frac{1}{G} \frac{2qL(W_c + H_c)}{Ah_{fg}} - \frac{c_{p,l}\Delta T_{sub}}{h_{fg}} \quad (38)$$

where  $c_{p,l}$  is the heat capacity of the liquid,  $\text{J}/(\text{kg}\cdot\text{K})$ ;  $W_c$  and  $H_c$  are the width and height of the channel, m. It is worth noting that  $x_{out}$  is another term of vapor quality  $\sigma$  to show relevance with inlet subcooling.  $x_{out}$  calculated at different  $N_{in}$  is presented in Figure 11.

Clearly,  $x_{out}$  characterizes the difference between the vaporization margin due to inlet subcooling and the heat absorbed by the fluid. The special cases of  $x_{out} = 0$  and  $x_{out} = 1$  lead to the minimum and maximum values of the characteristic length of two-phase flow in the channel (i.e.,  $L_{tp,min} = 0$  and  $L_{tp,max} = L$ ). Especially in cases of point a, b, c, and d in Figure 11 where  $x_{out} = 0$ , which corresponds to the vanishing of the two-phase flow region, the partial derivative of the outlet quality with respect to the mass flux is:

$$\left. \frac{\partial x_{out}}{\partial G} \right|_{x_{out}=0} = - \frac{(c_{p,l}\Delta T_{sub})^2}{qh_{fg}} \frac{A}{2L(W_c + H_c)} \quad (39)$$

This partial derivative, which is proportional to the square of the inlet subcooling, can be used to approximately characterize how drastically the two-phase flow region (Zone II) changes with mass flow rate. As  $N_{in}$  increases, the magnitude of this partial derivative rises, suggesting a steeper channel load curve in Zone II. Comparison of the slopes at points a, b, c, and d leads to the same conclusion. Since the entry effects significantly increase the pressure drop in Zone III while the pressure drop in Zone I remains almost constant, the channel load curve in Zone II is consistently flatter than that under the fully developed assumption at different  $N_{in}$ . Thus, the entry effects will accelerate the process of approaching the critical inlet subcooling.

Consider a microchannel whose load curve has a slope just greater than 0 in Zone II while decreasing inlet subcooling. A system consisting of such identical microchannels arranged

in parallel is assuredly stable, since there is no operating point with the same pressure drop among the three regions. At this junction, the inlet subcooling is defined as the critical subcooling mentioned earlier. Any inlet subcooling below this critical value can ensure stability and uniform flow distribution in parallel channel systems.

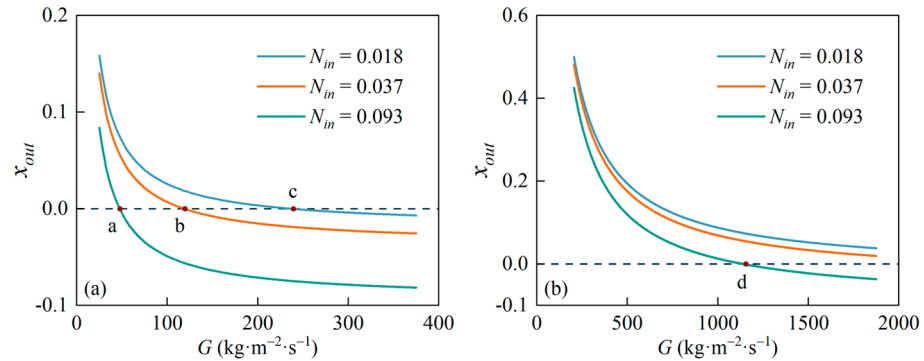


**Figure 11.** Thermodynamic quality  $x_{out}$  at the channel outlet under different heat fluxes: (a)  $q = 5 \text{ W/cm}^2$ ; (b)  $q = 120 \text{ W/cm}^2$ .

As heat flux increases from  $5 \text{ W/cm}^2$  to  $120 \text{ W/cm}^2$ , the entry effects can lead to a flatter curve in Zone II at the same  $N_{in}$ . Compared with the fully developed flow assumption, the parallel channel system can reach its critical subcooling at a higher  $N_{in}$ , thereby narrowing the range of inlet subcooling associated with flow instability. Detailed data are provided in Table 4.

**Table 4.** Critical subcooling at different heat fluxes.

	$q = 5 \text{ W}\cdot\text{cm}^{-2}$		$q = 120 \text{ W}\cdot\text{cm}^{-2}$	
	EE <sup>1</sup>	FDFA <sup>2</sup>	EE	FDFA
<b>Critical <math>N_{in}</math></b>	0.0044	0.0031	0.0121	0.0009
<b>Critical <math>\Delta T_{sub}</math> (K)</b>	2.5	1.8	6.6	0.6
<b>Expanding proportion</b>	38.89%		1000%	

<sup>1</sup> EE denotes the case considering entry effects. <sup>2</sup> FDFA denotes the case assuming fully developed flow.

For heat fluxes of  $5 \text{ W/cm}^2$  and  $120 \text{ W/cm}^2$ , entry effects can respectively increase the critical subcooling by 0.7 K and 6 K. Consequently, the range of inlet subcooling for system stability expands by 38.89% and 1000%, significantly widening the thermodynamic stable operating state.

#### 4. Conclusions

This study explores the impact of entry effects on Ledinegg instability and maldistribution within parallel microchannels, particularly those with small length-to-diameter ratios. Evaluations are conducted by utilizing a two-phase separated flow model and linearization analysis of system dynamics.

The entry effects increase the pressure drop, especially for the liquid phase, narrowing the possible flow rate range of the channel under a given pressure drop. Consequently, the total flow range of flow instability in parallel microchannels is also narrowed, since it mainly consists of specific combinations comprising liquid phase flow. For heat fluxes of  $5 \text{ W/cm}^2$  and  $120 \text{ W/cm}^2$ , the entry effects reduce the total flow rate range of flow instability by 4.73% and 47.52%, respectively, compared with the range under the fully developed flow assumption. Furthermore, the total flow rate range of flow maldistribution is decreased by 4.70% and 46.75%, respectively.

By analyzing the dimensionless boiling number and subcooling number, the stable thermodynamic operating range expands under the impact of the entry effects. When inlet subcooling decreases, the entry effects can accelerate the disappearance of two-phase flow

in the microchannel. For heat fluxes of  $5 \text{ W/cm}^2$  and  $120 \text{ W/cm}^2$ , the entry effects can raise the critical inlet subcooling by 0.7 K and 6 K and extend the range of inlet subcooling for stable operation by 38.89% and 1000%, respectively.

This study is carried out under conditions of thermal isolation between channels and only for a system consisting of two parallel channels, with the aim of exploring basic influence of entry effects on the properties of interest. With this primary research, we hope to initiate further studies by investigating thermally coupled microchannel scenarios and expanding the number of channels.

**Author Contributions:** Conceptualization, J.J., C.C., H.H. and Z.P.; methodology, J.J., C.C. and Z.P.; software, J.J. and C.C.; validation, J.J.; formal analysis, J.J.; investigation, J.J.; data curation, J.J.; writing—original draft preparation, J.J.; writing—review and editing, H.H. and Z.P. All authors have read and agreed to the published version of the manuscript.

**Funding:** This research received no external funding.

**Data Availability Statement:** Data are contained within the article.

**Conflicts of Interest:** Author Haoxiang Huang was employed by the company China Anhui Smagnet Materials Technology Co., Ltd. The re-remaining authors declare that the research was conducted in the absence of any commercial or financial relationships that could be construed as a potential conflict of interest.

## Nomenclature

$A$	cross-section area, $\text{m}^2$	<i>Greek symbols</i>	
$C$	empirical constant for $f_A$	$\alpha$	vapor volume fraction
$c_p$	heat capacity, $\text{J}/(\text{kg}\cdot\text{K})$	$\beta$	channel aspect ratio
$D$	hydraulic diameter, m	$\epsilon$	partial derivative
$F_w$	frictional pressure gradient	$\lambda$	eigenvalue
$f$	friction factor	$\mathbf{v}$	eigenvector
$G$	mass flux ( $W/A$ ), $\text{kg}/(\text{m}^2\cdot\text{s})$	$\rho$	density, $\text{kg}/\text{m}^3$
$H_c$	channel height, m	$\sigma$	vapor quality
$h$	specific enthalpy, $\text{J}/\text{kg}$	$\tau_w$	wall shear stress, Pa
$h_{fg}$	latent heat of vaporization, $\text{J}/\text{kg}$		
$K$	additional dimensionless pressure drop	<i>Subscript</i>	
$k$	stability criterion	$A$	apparent
$L$	channel length, m	$apx$	approximate
$m$	inertia coefficient	$e$	entrance region
$N$	dimensionless number	$f$	liquid
$P$	pressure head/drop, Pa	$g$	vapor
$P^*$	dimensionless pressure drop	$i$	channel number
$P_T$	power input, W	$in$	inlet
$p$	pressure, Pa	$out$	outlet
$Q$	volume flow rate, ml/min	$p$	pump
$q'$	heat input per unit length, $\text{W}/\text{m}$	$pch$	phase change
$q$	heat flux, $\text{W}/\text{m}^2$	$sub$	subcooling
$R$	flow rate fraction	$tp$	two-phase flow
$Re$	Reynolds number		
$S$	slip ratio		
$T$	temperature, K		
$t$	time coordinate		
$u$	velocity, m/s		
$v$	specific volume, $\text{m}^3/\text{kg}$		
$W$	mass flow rate, $\text{mg}/\text{s}$		
$W_c$	channel width, m		
$x$	axial position, m		
$x_{out}$	thermodynamic quality		
$x^*$	channel length-to-diameter ratio		
$x^+$	dimensionless hydrodynamic length		

## References

1. Yu, H.; Li, T.; Zeng, X.; He, T.; Mao, N. A Critical Review on Geometric Improvements for Heat Transfer Augmentation of Microchannels. *Energies* **2022**, *15*, 9474. [[CrossRef](#)]
2. ElFaham, M.; Tang, C.C. A Comparative Analysis of Two-Phase Flow Boiling Heat Transfer Coefficient and Correlations for Hydrocarbons and Ethanol. *Energies* **2023**, *16*, 5931. [[CrossRef](#)]
3. Jiang, Z.; Song, M.; Shen, J.; Zhang, L.; Zhang, X.; Lin, S. Experimental Investigation on the Flow Boiling of Two Microchannel Heat Sinks Connected in Parallel and Series for Cooling of Multiple Heat Sources. *Micromachines* **2023**, *14*, 1580. [[CrossRef](#)] [[PubMed](#)]
4. O'Neill, L.E.; Mudawar, I. Review of two-phase flow instabilities in macro- and micro-channel systems. *Int. J. Heat Mass Transf.* **2020**, *157*, 119738. [[CrossRef](#)]
5. Ledinegg, M. Instability of flow during natural and forced circulation. *Die Wärme* **1938**, *61*, 891–898.
6. Kakac, S.; Bon, B. A Review of two-phase flow dynamic instabilities in tube boiling systems. *Int. J. Heat Mass Transf.* **2008**, *51*, 399–433. [[CrossRef](#)]
7. Akagawa, K.; Kono, M.; Sakaguchi, T.; Nishimura, M. Study on Distribution of Flow Rates and Flow Stabilities in Parallel Long Evaporators. *Bull. JSME* **1971**, *14*, 837–848. [[CrossRef](#)]
8. Manavela Chiapero, E.; Doder, D.; Fernandino, M.; Dorao, C.A. Experimental parametric study of the pressure drop characteristic curve in a horizontal boiling channel. *Exp. Therm. Fluid Sci.* **2014**, *52*, 318–327. [[CrossRef](#)]
9. Oh, C.H.; Chapman, J.C. Two-phase flow instability for low-flow boiling in vertical uniformly heated thin rectangular channels. *Nucl. Technol.* **1996**, *113*, 327–337. [[CrossRef](#)]
10. Aritomi, M.; Aoki, S.; Inoue, A. Instabilities in parallel channel of forced-convection boiling upflow system, (II) Experimental results. *J. Nucl. Sci. Technol.* **1977**, *14*, 88–96. [[CrossRef](#)]
11. Guo, Y.; Xia, G.; Zeng, H.; Hu, M. Instability in Parallel Channel System. In Proceedings of the ASME 2010 3rd Joint US-European Fluids Engineering Summer Meeting Collocated with 8th International Conference on Nanochannels, Microchannels, and Minichannels, Montreal, QC, Canada, 1–5 August 2010; pp. 1945–1949.
12. Zhang, T.; Tong, T.; Chang, J.-Y.; Peles, Y.; Prasher, R.; Jensen, M.K.; Wen, J.T.; Phelan, P. Ledinegg instability in microchannels. *Int. J. Heat Mass Transf.* **2009**, *52*, 5661–5674. [[CrossRef](#)]
13. Thiagarajan, N. Experimental Investigation of Thermo-Hydraulic Characteristics of Two-Phase Flow of FC72 in Microchannel Heat Sinks. Master's Thesis, Auburn University, Auburn, AL, USA, 2009.
14. Ding, Y. Experimental Investigation of Two-Phase Flow Phenomena in Horizontal Convective In-Tube Boiling System. Ph.D. Thesis, University of Miami, Miami, FL, USA, 1994.
15. Maulbetsch, J.S.; Griffith, P. *A Study of System-Induced Instabilities in Forced-Convection Flows with Subcooled Boiling*; Massachusetts Institute of Technology: Cambridge, MA, USA, 1965.
16. Martinelli, R.C.; Nelson, D.B. Prediction of Pressure Drop During Forced-Circulation Boiling of Water. *Trans. Am. Soc. Mech. Eng.* **1948**, *70*, 695–702. [[CrossRef](#)]
17. Lockhart, W.R. Proposed Correlation of Data for Isothermal Two-Phase, Two-Component Flow in Pipes. *Chem. Eng. Prog.* **1949**, *45*, 39–48.
18. Mishima, K.; Hibiki, T. Some characteristics of air-water two-phase flow in small diameter vertical tubes. *Int. J. Multiph. Flow* **1996**, *22*, 703–712. [[CrossRef](#)]
19. Muzychka, Y.S.; Awad, M.M. Asymptotic Generalizations of the Lockhart–Martinelli Method for Two Phase Flows. *J. Fluids Eng.* **2010**, *132*, 031302. [[CrossRef](#)]
20. Mekheimer, K.S.; Shankar, B.M.; Ramadan, S.F.; Mallik, H.E.; Mohamed, M.S. On the Stability of Convection in a Non-Newtonian Vertical Fluid Layer in the Presence of Gold Nanoparticles: Drug Agent for Chemotherapy. *Mathematics* **2021**, *9*, 1302. [[CrossRef](#)]
21. Mekheimer, K.S.; Shankar, B.M.; Abo-Elkhair, R.E. Effects of Hall current and permeability on the stability of peristaltic flow. *SN Appl. Sci.* **2019**, *1*, 1610. [[CrossRef](#)]
22. Hasan, A.A.; Mekheimer, K.S.; Tantawy, B.E. Self-gravitating stability of resistive streaming triple superposed of fluids layers under the influence of oblique magnetic fields. *Int. J. Appl. Electromagn. Mech.* **2020**, *63*, 409–419. [[CrossRef](#)]
23. Reich, S. On the local qualitative behavior of differential-algebraic equations. *Circuits Syst. Signal Process.* **1995**, *14*, 427–443. [[CrossRef](#)]
24. Van Oevelen, T.; Weibel, J.A.; Garimella, S.V. Predicting two-phase flow distribution and stability in systems with many parallel heated channels. *Int. J. Heat Mass Transf.* **2017**, *107*, 557–571. [[CrossRef](#)]
25. Rosa, P.; Karayiannis, T.G.; Collins, M.W. Single-phase heat transfer in microchannels: The importance of scaling effects. *Appl. Therm. Eng.* **2009**, *29*, 3447–3468. [[CrossRef](#)]
26. Zivi, S.M. Estimation of Steady-State Steam Void-Fraction by Means of the Principle of Minimum Entropy Production. *J. Heat Transf.* **1964**, *86*, 247–251. [[CrossRef](#)]
27. Acrivos, A.; Babcock, B.D.; Pigford, R.L. Flow distributions in manifolds. *Chem. Eng. Sci.* **1959**, *10*, 112–124. [[CrossRef](#)]
28. Shah, R.K.; London, A.L. Chapter VII—Rectangular Ducts. In *Laminar Flow Forced Convection in Ducts*; Academic Press: New York, NY, USA, 1978; pp. 196–222.
29. Shah, R.K. A Correlation for Laminar Hydrodynamic Entry Length Solutions for Circular and Noncircular Ducts. *J. Fluids Eng.* **1978**, *100*, 177–179. [[CrossRef](#)]

30. Shapiro, A.H.; Siegel, R.; Kline, S.J. Friction factor in the laminar entry region of a smooth tube. *J. Appl. Mech. Trans. ASME* **1954**, *21*, 289.
31. Bender, E. Druckverlust bei laminarer Strömung im Rohreinlauf. *Chem. Ing. Tech.* **1969**, *41*, 682–686. [[CrossRef](#)]
32. Curr, R.M.; Sharma, D.; Tatchell, D.G. Numerical predictions of some three-dimensional boundary layers in ducts. *Comput. Methods Appl. Mech. Eng.* **1972**, *1*, 143–158. [[CrossRef](#)]
33. Duan, Z.; Ma, H. Chapter Four—Pressure drop and heat transfer in the entrance region of microchannels. In *Advances in Heat Transfer*; Abraham, J.P., Gorman, J.M., Minkowycz, W.J., Eds.; Elsevier: Amsterdam, The Netherlands, 2020; Volume 52, pp. 249–333.
34. Junemo, K.; Clement, K. Liquid flow in microchannels: Experimental observations and computational analyses of microfluidics effects. *J. Micromech. Microeng.* **2003**, *13*, 568. [[CrossRef](#)]
35. Miglani, A.; Weibel, J.A.; Garimella, S.V. Measurement of flow maldistribution induced by the Ledinegg instability during boiling in thermally isolated parallel microchannels. *Int. J. Multiph. Flow* **2021**, *139*, 103644. [[CrossRef](#)]
36. Mirmanto, M.; Kenning, D.; Lewis, J.; Karayiannis, T. Pressure drop and heat transfer characteristics for single-phase developing flow of water in rectangular microchannels. *J. Phys. Conf. Ser.* **2012**, *395*, 2085. [[CrossRef](#)]
37. Chiapero, E.M.; Fernandez, M.; Dorao, C. Parametric study of the pressure characteristic curve in a boiling channel. *Comput. Therm. Sci.* **2011**, *3*, 157–168. [[CrossRef](#)]

**Disclaimer/Publisher’s Note:** The statements, opinions and data contained in all publications are solely those of the individual author(s) and contributor(s) and not of MDPI and/or the editor(s). MDPI and/or the editor(s) disclaim responsibility for any injury to people or property resulting from any ideas, methods, instructions or products referred to in the content.